Cryo-reconstructions of P22 polyheads suggest that phage assembly is nucleated by trimeric interactions among coat proteins

2010 Phys. Biol. 7 045004

(http://iopscience.iop.org/1478-3975/7/4/045004)

Phys. Biol. **7** (2010) 045004 (14pp) doi:10.1088/1478-3975/7/4/045004

Cryo-reconstructions of P22 polyheads suggest that phage assembly is nucleated by trimeric interactions among coat proteins

Kristin N Parent[1], Robert S Sinkovits[1,4], Margaret M Suhanovsky[2], Carolyn M Teschke[2], Edward H Egelman[3] and Timothy S Baker[1,5,6]

[1] Department of Chemistry & Biochemistry, University of California, San Diego, La Jolla, CA, USA
[2] Department of Molecular and Cell Biology, University of Connecticut, Storrs, CT, USA
[3] Department of Biochemistry and Molecular Genetics, University of Virginia, Charlottesville, VA, USA
[4] San Diego Supercomputer Center, University of California, San Diego, La Jolla, CA, USA
[5] Division of Biological Sciences, University of California, San Diego, La Jolla, CA, USA

E-mail: tsb@ucsd.edu

Received 29 April 2010
Accepted for publication 1 July 2010
Published 9 December 2010
Online at stacks.iop.org/PhysBio/7/045004

Abstract

Bacteriophage P22 forms an isometric capsid during normal assembly, yet when the coat protein (CP) is altered at a single site, helical structures (polyheads) also form. The structures of three distinct polyheads obtained from F170L and F170A variants were determined by cryo-reconstruction methods. An understanding of the structures of aberrant assemblies such as polyheads helps to explain how amino acid substitutions affect the CP, and these results can now be put into the context of CP pseudo-atomic models. F170L CP forms two types of polyhead and each has the CP organized as hexons (oligomers of six CPs). These hexons have a skewed structure similar to that in procapsids (precursor capsids formed prior to dsDNA packaging), yet their organization differs completely in polyheads and procapsids. F170A CP forms only one type of polyhead, and though this has hexons organized similarly to hexons in F170L polyheads, the hexons are isometric structures like those found in mature virions. The hexon organization in all three polyheads suggests that nucleation of procapsid assembly occurs via a trimer of CP monomers, and this drives formation of a $T = 7$, isometric particle. These variants also form procapsids, but they mature quite differently: F170A expands spontaneously at room temperature, whereas F170L requires more energy. The P22 CP structure along with scaffolding protein interactions appear to dictate curvature and geometry in assembled structures and residue 170 significantly influences both assembly and maturation.

Abbreviations

3D	three-dimensional
CP	coat protein
cryo-TEM	cryo-transmission electron microscopy
gp	gene product
IHRSR	iterative helical real space reconstruction method
WT	wild type

[6] Author to whom any correspondence should be addressed.

Introduction

The capsids of many icosahedral viruses assemble from viral protein subunits that are organized as penton and hexon

morphological units ('capsomers'). Pentons are generally pentamers and hexons are either hexamers or trimers of the major coat protein (CP) [1]. Viral morphogenesis does not always result in the formation of infectious particles but sometimes yields aberrant, off-pathway products such as polyheads. These are non-infectious, long, tubular structures that primarily arise from mutation in one or more genes that encode for head proteins or a change in assembly conditions (e.g. pH or ionic strength). The CPs of bacteriophages T7 [2], T4 [3], SPO1 [4] and λ [5], and also cowpea chlorotic mottle virus [6] and the human immunodeficiency virus [7, 8] form polyheads comprising hexons. Though less prevalent, tubular, polyhead-like assemblies can form from pentons as happens with polyomavirus VP1 [9] or from dimers of VP6 trimers in rotavirus [10].

Assembly of bacteriophage P22 *in vivo* [11] proceeds through a nucleation-limited reaction in which 60–300 scaffolding proteins (gene product 8: gp8) co-polymerize with 415 copies of monomeric CPs, a dodecamer of portal proteins (gp1) and 12–20 copies each of three ejection proteins (gp7, gp16 and gp20) to form procapsids. The P22 procapsid shell is an isometric structure composed of the portal complex and 71 capsomers of CPs, 60 of which are skewed hexons and 11 of which are symmetric pentons. Virus maturation begins when a complex of two additional proteins (gp2/3) packages the dsDNA genome while scaffolding proteins are released. This process is accompanied by an ∼10% expansion in head volume, a large-scale regularization of the hexons into sixfold symmetric units and a transformation of the capsid from a roughly spherical to a polyhedral morphology. The final stage of assembly involves addition of the tail, which includes the tail plug proteins, gp4 (12 copies) and gp10 (6 copies), the tail needle protein, gp26 (3 copies), and the tailspike protein, gp9 (18 copies).

Scaffolding proteins are required both *in vivo* and *in vitro* for 'proper' P22 assembly (i.e. that leads to native, infectious particles or those that closely resemble them structurally). Assembly goes awry if scaffolding protein is absent or if its gene is mutated, and results in the production of aberrant particles such as petites and giants (icosahedral structures with triangulation symmetries other than $T = 7$), and 'spirals' [12]. Scaffolding proteins also play a critical role in preventing the formation of P22 polyheads. To date, polyheads have only been observed to occur when the P22 CP contains a variation at residue F170, and polyhead formation depends both on the interactions with scaffolding proteins and also the structure of the CP [13, 14]. We have recently derived a pseudo-atomic model of the 430-residue (∼47 kDa), P22 CP that shows it has an HK97-like core and a surface-exposed telokin domain (figure 1(*a*)) [15]. In addition, a four-strand β-sheet ('β-hinge'), which connects the A-domain to the core and includes residue F170, is proposed to play a crucial role during P22 morphogenesis (figure 1(*b*)) [11]. Three variations within the β-hinge (F170L, F170A and F170K) induce CPs to assemble into polyheads and this abortive assembly pathway is affected by the presence or absence of scaffolding proteins and their binding affinities to the different CPs [14].

A recent study with the F170L CP variant has demonstrated that polyhead formation with this variant only occurs when scaffolding proteins are absent [14]. This study also showed that F170A and F170K variants display more severe assembly defects than F170L, since polyheads form from these CPs even in the presence of scaffolding proteins [14]. Affinity chromatography and scaffolding re-entry experiments revealed that the strength of CP interaction with scaffolding proteins differs between WT and variant CPs. Indeed, WT CPs have the strongest interactions with scaffolding proteins, followed by F170L and F170K, with F170A being the weakest. Despite these noticeable differences, infections with phage containing each of the F170 variant CPs can still lead to assembly of some infectious particles, indicating that proper assembly occurs even when scaffolding:CP affinity is lower than normal [13, 14]. Three-dimensional (3D) cryo-reconstructions computed from images of vitrified, F170 variant procapsids assembled *in vivo*, display skewed hexons with a morphology that is very similar to what is seen in WT procapsids [14]. However, difference map analyses show that F170A and F170K pentons differ from the pentons in WT and F170L procapsids, owing to increased CP rigidity [14].

Scaffolding proteins are clearly important for recruiting variant CPs into hexon and penton subunit forms to form functional structures. The putative scaffolding protein-binding site on the CP maps to the inner surface of the procapsid shell at the icosahedral and quasi threefold axes of symmetry [16, 17]. Curiously, residue 170 in the pseudo-atomic model of the P22 CP lies quite distant from these axes and from the inner shell surface (figure 1(*c*)) [15]. This raises the question of how F170 substitutions affect CP:scaffolding protein interactions during assembly and promote polyhead formation.

We have used cryo-transmission electron microscopy (cryo-TEM) and the iterative helical real space reconstruction (IHRSR) method [18] to examine the structures of P22 polyheads formed from F170L and F170A CP variants. Polyheads consist of CP capsomers organized as helical arrays. A helical assembly, in which all asymmetric units are in an equivalent environment, can be described as having a combination of a screw symmetry (a coupled rotation about the axis and translation parallel to the axis) and a rotational symmetry about the axis, characterized by a cyclic point group symmetry C_n. Here we characterize three classes of polyhead, each displaying a different rotational (C_n) symmetry. F170L CP formed polyheads with C_9 and C_1 symmetries, whereas F170A CP only formed polyheads with C_3 symmetry. Notwithstanding these different symmetries, all three polyheads solely comprise CP hexamers that resemble hexons either in procapsids if the CP variant is F170L, or in mature virions if the CP variant is F170A. Also, the arrangements of hexons in these three types of polyheads are quite distinct from those in the CP shells of isometric, native procapsids and virions. Hence, sometime early in assembly, scaffolding proteins appear to directly establish or influence CP intersubunit and interhexon interactions and this affects the geometry and curvature of the resulting products.

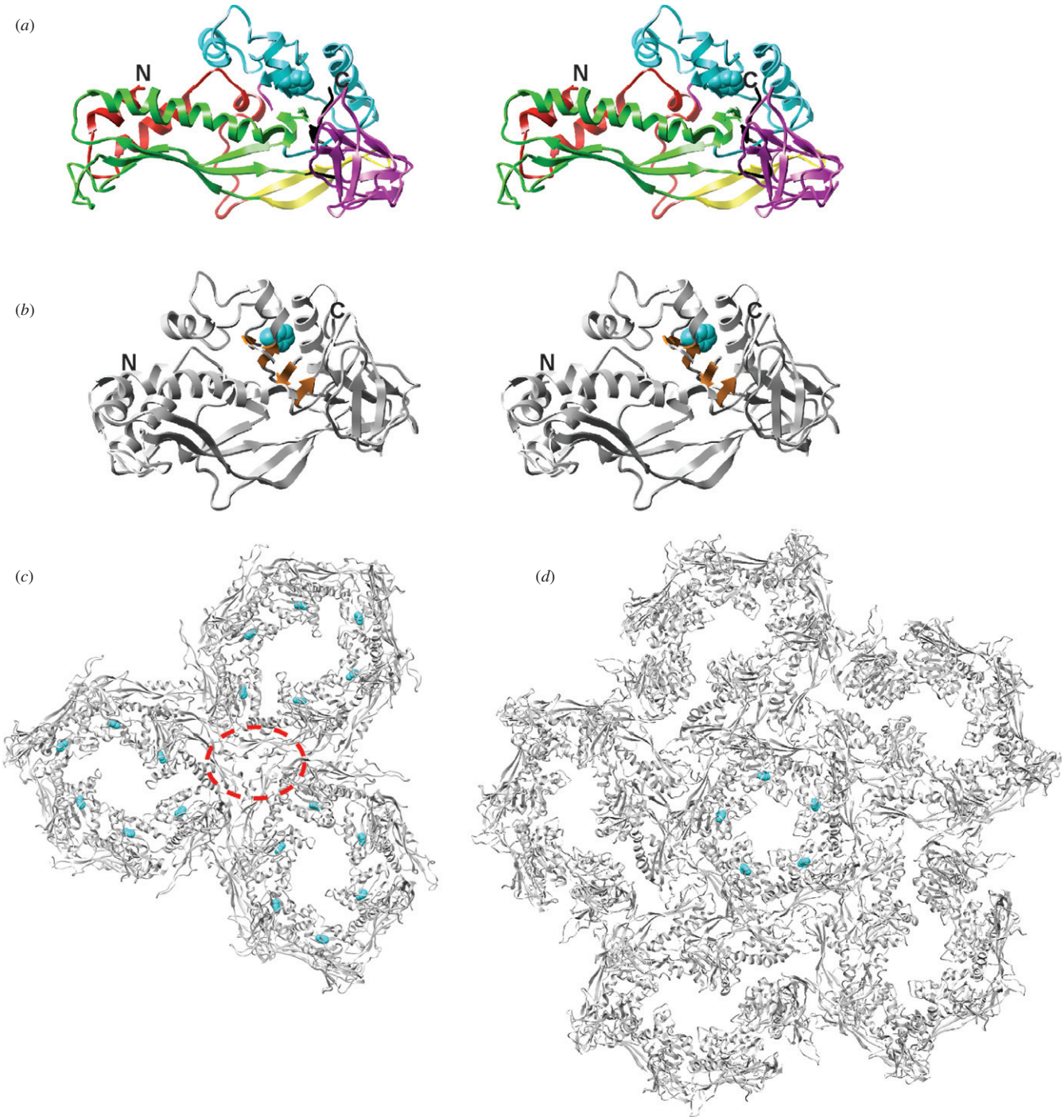

Figure 1. P22 subunit structure and location of residue 170. (*a*) Stereo image of one CP from the WT procapsid state (PDB accession number 3IYI) with color-coded domains: N-arm (red), E-loop (yellow), P-domain (green), A-domain (cyan), telokin domain (magenta), the last modeled 15 residues of the C-terminus (black) [11]. A van der Waals representation of the side chain of F170 is highlighted in cyan. (*b*) Same as (*a*), but with the backbone uncolored, the β-hinge in orange, and with the model rotated 25° anti-clockwise about a vertical axis. (*c*) Three adjacent hexons, viewed from outside the capsid along a strict threefold axis. The putative scaffolding binding site on the inside of the capsid is identified by the red, dashed oval [16, 17]. (*d*) One penton and adjacent five hexons viewed along a fivefold axis. In panels (*c*) and (*d*), the WT CP is rendered as gray ribbons, and F170 as in (*a*).

Materials and methods

Preparation and purification of F170A procapsid shells

Salmonella typhimurium serovar typhii strain DB7136 (leuA414am, hisC525am, su°) expressing CPs from mutated pHBW1 were infected with P22 phage carrying amber mutations in gene 5 to stop production of phage-encoded CPs, and genes 2 and 13 to prevent dsDNA packaging and cell lysis, respectively. The P22 strain also carried the c1–7 allele to prevent lysogeny. Procapsid purification and production of shells were carried out for F170A CP as described previously [14]. F170A polyheads were co-purified with procapsids.

In vitro F170L polyhead production

Samples (1 mg mL^{-1}) of F170L procapsid shells were dissociated and the CP unfolded with 6.75 M urea in 20 mM sodium phosphate buffer (pH 7.6) for 30 min at room temperature. Refolding of the F170L CP monomers was initiated by dialysis until equilibrium against 20 mM sodium phosphate buffer (pH 7.6) at 4 °C. Polyheads were generated by concentrating the refolded F170L monomers to ∼35 mg mL^{-1} with a YM-10 Centricon at 6450 rpm and 4 °C.

Cryo-TEM

Small (3.5 μL) aliquots of purified polyheads (F170L at ∼35 mg mL^{-1} and F170A at ∼8 mg mL^{-1}) were vitrified and examined using established procedures [19]. Briefly, polyhead samples were applied to homemade lacey carbon grids (F170L) or holey (Quantifoil) grids (F170A) that had been glow-discharged for ∼15 s in an Emitech K350 evaporation unit. Grids were then blotted with Whatman filter paper for ∼5 s, plunged into liquid ethane, and transferred into a precooled, FEI Polara, multi-specimen holder, which maintained the specimen at liquid nitrogen temperature. Micrographs were either recorded on a Gatan 4K^2 CCD camera or on Kodak SO-163 electron-image film at 200 keV in an FEI Polara microscope under minimal-dose conditions (∼15 e Å^{-2}) at nominal magnifications of 79 000× (CCD, 1.88 Å per pixel) and 39 000 × (film, 1.62 Å per pixel when digitized at 6.35 μm on a Nikon Supercool 8000). (A representative micrograph of the F170A sample is shown in figure 6.) Additional data collection statistics, including the range of objective lens defocus settings used to record each set of polyhead micrographs, are listed in table 1. The program RobEM (http://cryoEM.ucsd.edu/programs.shtm) was used to estimate the level of defocus and astigmatism for each micrograph.

Particle boxing, preprocessing and IHRSR reconstruction

The helixboxer routine in EMAN [20] was used to extract individual polyheads from CCD images (F170L) or digitized film data (F170A) that displayed minimum astigmatism and specimen drift. Each boxed image was padded out to 8192^2 pixels with the background value set equal to the average pixel density along the original border of the boxed image. A computed diffraction pattern, generated for each polyhead image using SPIDER [21], enabled us to systematically index the layer lines and sort the polyheads into distinct classes (figure 2). Each polyhead image was cut into several overlapping segments whose lengths and overlap distances are listed in table 1. These segments were further classified on the basis of polyhead diameter, which was estimated by creating a twofold binned, low-pass filtered (to 1/20 Å^{-1}) version of each image segment and projecting that parallel to the helix axis to form a one-dimensional density profile. The distance between the two most prominent, well-separated peaks in the density profile was used as the estimate of the polyhead diameter for that segment (figure 3(*a*)).

Table 1. IHRSR++ statistics.

CP variant	F170L	F170L	F170A
Cyclic symmetry (C_n)	C_9	C_1	C_3
Image recording media	CCD	CCD	Film
Pixel size (Å)	1.88	1.88	1.62
Objective lens defocus range (μm)	0.91–4.96	1.14–3.39	1.10–3.56
Total no. of micrographs recorded[a]	713	713	233
Total no. of boxed polyheads[a]	1141	1141	331
No. of polyheads used in cryo-reconstructions	187	63	16
No. of segments	2958	7433	2670
Segment length (pixels)	300	100	400
Shift between segments (pixels)[b]	60	6	25
Padded segment size (pixels)	360	360	440
Range of initial $\Delta\varphi$ (degrees)[c]	15–25	36–38	31–34
Refined value of $\Delta\varphi$ (degrees)	19.0	37.4	32.3
Range of initial ΔZ (Å)[c]	95–120	6–12	29–33
Refined value of ΔZ (Å)	104.0	10.5	31.5
Smallest diameter (Å)	305	313	411
Largest diameter (Å)	418	444	518

[a] These numbers cited are the initial total data set collected for F107L since both types of polyhead were present in the same sample.
[b] The shift between segments is dictated by the helical symmetry and is generally set larger than the axial rise per subunit [67].
[c] Initial ranges listed include starting values that yielded correct structures.

The diameters measured for the polyheads included in each class varied over different ranges (more for F170L than for F170A) (figure 3). In both types of F170L polyhead, a reconstruction computed from the entire set of image segments for that class led to a map with unrecognizable hexons. This most likely resulted because some of the included segments were from portions of polyheads that were distorted and deviated from the idealized helical lattice. In addition to diffraction pattern quality, we used polyhead diameter as a second metric to identify segments to omit from the image reconstructions. To derive the final reconstructions presented here, we computed multiple reconstructions for each polyhead class by systematically excluding segments based on diameter and removing these from subsequent reconstructions if the appearance of the map, incoherent average of the power spectra (see below) and reconstruction statistics improved (figure 3, table 1) (data not shown). Careful inspection of these reconstructions showed that the clarity of most features (e.g. CP hexons) steadily improved until the noise level began to increase owing to the use of too few segments. We also used an additional metric for selecting particles, in which the signal to noise ratio in the incoherent sum of the power spectra from included segments was monitored. Increased layer line intensities and emergence of layer lines at higher spatial frequencies with successive reconstructions, computed as described above, indicated a level of self-consistency in the segments selected for inclusion in the final reconstructions (figure 2).

Before each polyhead reconstruction was computed, all included image segments were adjusted to correct for the phase reversals caused by the microscope contrast transfer

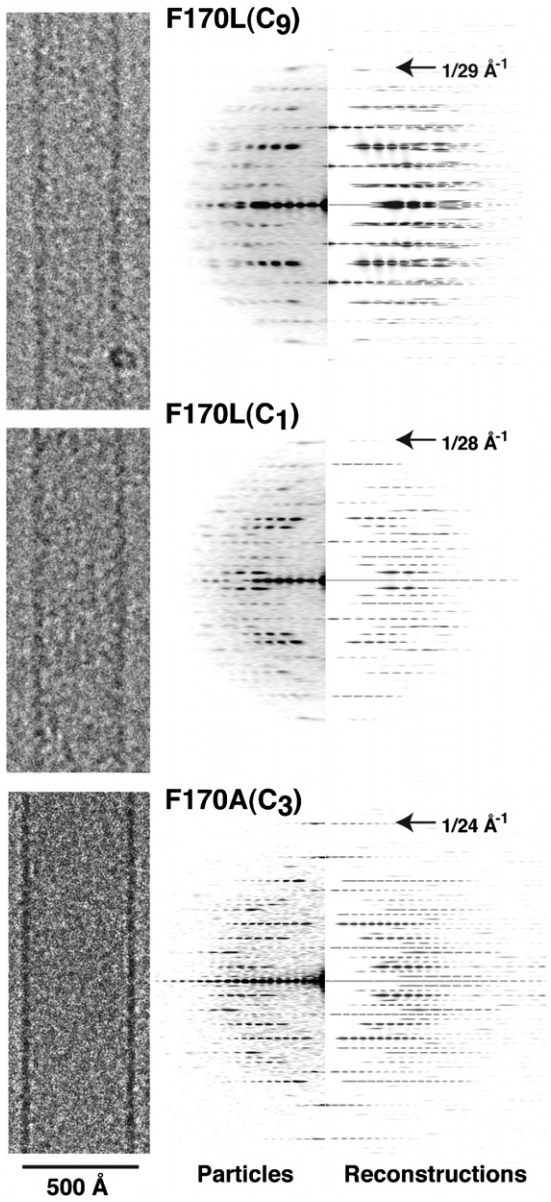

Figure 2. P22 polyhead images and diffraction patterns. Left column: representative images of vitrified samples of F170L C_9 (top), F170L C_1 (middle) and F170A C_3 (bottom). These C_1 and C_9 polyhead images were obtained from the same micrograph. Middle column: incoherently averaged power spectra of all images of each symmetry class used in the final reconstructions. All three polyheads display unique diffraction patterns. Right column: transforms of 2D projections of the reconstructed maps show good agreement with the averaged power spectra from the raw data.

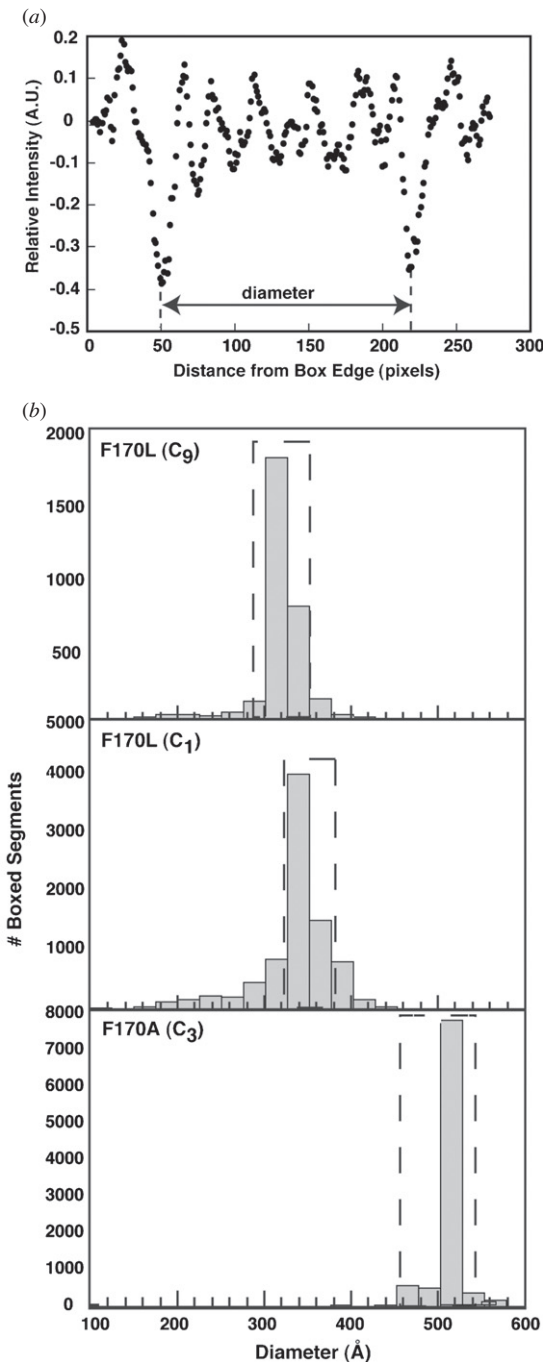

Figure 3. Measurement of polyhead diameters. (*a*) Diameter estimate made from a single segment of an F170L C_9 polyhead (see the Materials and methods section). (*b*) Plots of the measured segment diameters for all three symmetry classes. The C_9 and C_3 polyheads both exhibit much smaller variations in diameter relative to the C_1 form. Boxed areas indicate the diameters of the segments included in each final reconstruction.

function. Reconstructions were computed using IHRSR++ (version 1.4), which is an enhanced version of IHRSR [18] that additionally permits application of dihedral symmetry, search for out-of-plane tilt and construction of random models [22]. The starting model was either a smooth, featureless cylinder of approximately the correct inner and outer radii or a random model that had been constructed from the experimental images by assigning random orientations to the cylindrical coordinate angle, φ, and assuming that particles are properly centered within the box. Both methods for producing a starting model led to consistent reconstructions. The incoherent averages of the power spectra corresponding to each diffraction type and estimates of the polyhead diameters (described above) together provided sufficient data to derive initial values for the rotation ($\Delta\varphi$) and the axial rise (ΔZ) per subunit for each helical form. These were used as input to IHRSR++ but, in addition, multiple seed values for iterative refinement of the

$\Delta\varphi$ and ΔZ helical parameters for each class of polyhead were tested, and all led to consistent solutions (table 1). Such self-consistency argued that the correct helical lattices had been identified and persisted among the chosen segments. Also, for each data set, several different C_n symmetries were applied, but in each instance only one yielded a readily interpretable map with recognizable hexons.

Each final cryo-reconstruction was multiplied by the weighted average of the inverse CTF squared ($\langle 1/\mathrm{CFT}(\nu)^2\rangle$), where ν denotes the spatial frequency, with weighting being proportional to the number of polyhead segments at each defocus value. Adjustments to this correction were made to avoid overemphasis of contributions from the lowest spatial frequencies. Specifically, $\langle 1/\mathrm{CFT}(\nu)^2\rangle$ was averaged over all spatial frequencies and the lowest spatial frequency, ν', where $\langle 1/\mathrm{CFT}(\nu)^2\rangle$ first exceeds this value was identified. The correction for $\nu < \nu'$ was replaced with this averaged value.

The absolute hand of each F170L polyhead reconstruction was set to make the skew of the hexons the same as in procapsids. The handedness of the F170A polyhead was determined by recognizing obvious asymmetry in the capsid subunit morphology that is apparent in polyhead and isometric particle reconstructions (figures 4(*a*), (*b*) and 6(*c*)). Fourier shell correlation criteria [23] showed that all three polyhead cryo-reconstructions were reliable to at least 25 Å resolution. However, owing to the limited number of micrographs and particles used to compute the reconstructions, these criteria yielded an unrealistic measure of the map quality. We therefore estimated map resolution by comparing corresponding features in the polyhead and isometric particle reconstructions. By this means we estimated the resolutions of the C_9, C_1 and C_3 polyhead maps to be approximately 13, 13 and 11 Å, respectively. All software and data pre-processing scripts used to obtain the helical structures are accessible at http://cryoem.ucsd.edu/programs.shtm.

3D cryo-reconstruction of icosahedral F170A procapsid shells

A total of 187 micrographs exhibiting minimal astigmatism and specimen drift were selected for further processing and digitized as described above. The program RobEM was used to estimate the defocus of each micrograph (ranging between 0.65 and 5.68 μm), extract 1116 individual particle images and preprocess these images as described previously [19]. A subset of 150 particle images was used as input to the random-model computation procedure to generate an initial 3D density map at an ~25 Å resolution [22]. This map was then used to initiate determination and refinement of particle orientations and origins for the complete set of images using version 3.14 of AUTO3DEM [24]. Phases but not amplitudes of the particle structure factor data were corrected to compensate for the effects caused by the microscope contrast-transfer function [25]. The Fourier shell correlation criterion ($\mathrm{FSC}_{0.5}$) was used to estimate the resolution of the F170A icosahedral 3D reconstruction (17.1 Å) [23]. Graphical representations were generated with the RobEM and Chimera [26] visualization software packages.

Heat expansion of procapsids

Procapsid samples (1 mg mL^{-1}) were incubated for 15 min in a BIO-RAD MyCycler thermalcycler at temperatures ranging from 40 to 73 °C, after which they were placed on ice and diluted with ice-cold agarose sample buffer (0.25% bromophenol blue and 50% glycerol in TAE buffer; 40 mM Tris acetate and 1 mM EDTA). Agarose gel electrophoresis was performed in TAE buffer. Approximately 5 μg of protein was loaded in each lane of a 1.0% SeaKem agarose gel (modified from [27]). The gel was run at 100 V for 45 min at room temperature and stained with Coomassie blue.

Results and discussion

F170L and F170A CPs form three different classes of P22 polyhead

F170A polyheads were isolated from phage-infected cells and purified using a standard procapsid purification method [28]. F170L polyheads also form *in vivo* in the absence of scaffolding proteins, but they form much more efficiently *in vitro* [14]. Hence, we prepared F170L polyheads by concentrating refolded monomers to ~35 mg mL^{-1} at 4 °C (see the Materials and methods section) to produce sufficient quantities for cryo-TEM studies. Refolded, *in vitro*-assembled WT CPs form structures with the same morphology as those formed *in vivo* [28]. Furthermore, refolded and assembled F170L CPs also form some procapsids that are indistinguishable from WT procapsids (data not shown) and this implies that the refolded F170L CPs also adopt a biologically relevant structure. All polyheads were vitrified and imaged at 200 keV under standard, minimal dose conditions [19]. They appeared as relatively straight, thin-walled, hollow tubes with coarse surface features and ranged in length from ~140 to 800 nm (F170L) and up to as long as ~2 μm (F170A). Some F170L and F170A polyheads were capped at one or both ends [14]. Thus far we have been unable to purify and image F170K polyheads because they readily dissociate [14]. The F170L polyhead images yielded two distinct diffraction patterns that subsequently could be indexed as arising from helical arrays with either C_9 or C_1 cyclic symmetry (figure 2). In contrast, F170A polyheads only produced diffraction patterns consistent with C_3 symmetry (figure 2). Polyhead images that did not produce diffraction patterns with distinct layer lines, owing to inherent disorder along the length of the polyhead, were not included in the 3D reconstructions.

Each polyhead image in a given class was subdivided into several overlapping segments and the diameter of each segment was measured as described earlier (see the Materials and methods section). Only those segments within a narrow diameter range were used in the final reconstruction of each type of polyhead (figure 3). Some of the observed variability in the measured diameters may reflect errors in the actual estimations as might result from differences in micrograph contrast, defocus and noise levels, and in segment length. However, this method provided one useful metric for screening particle images. We used a systematic, empirical approach

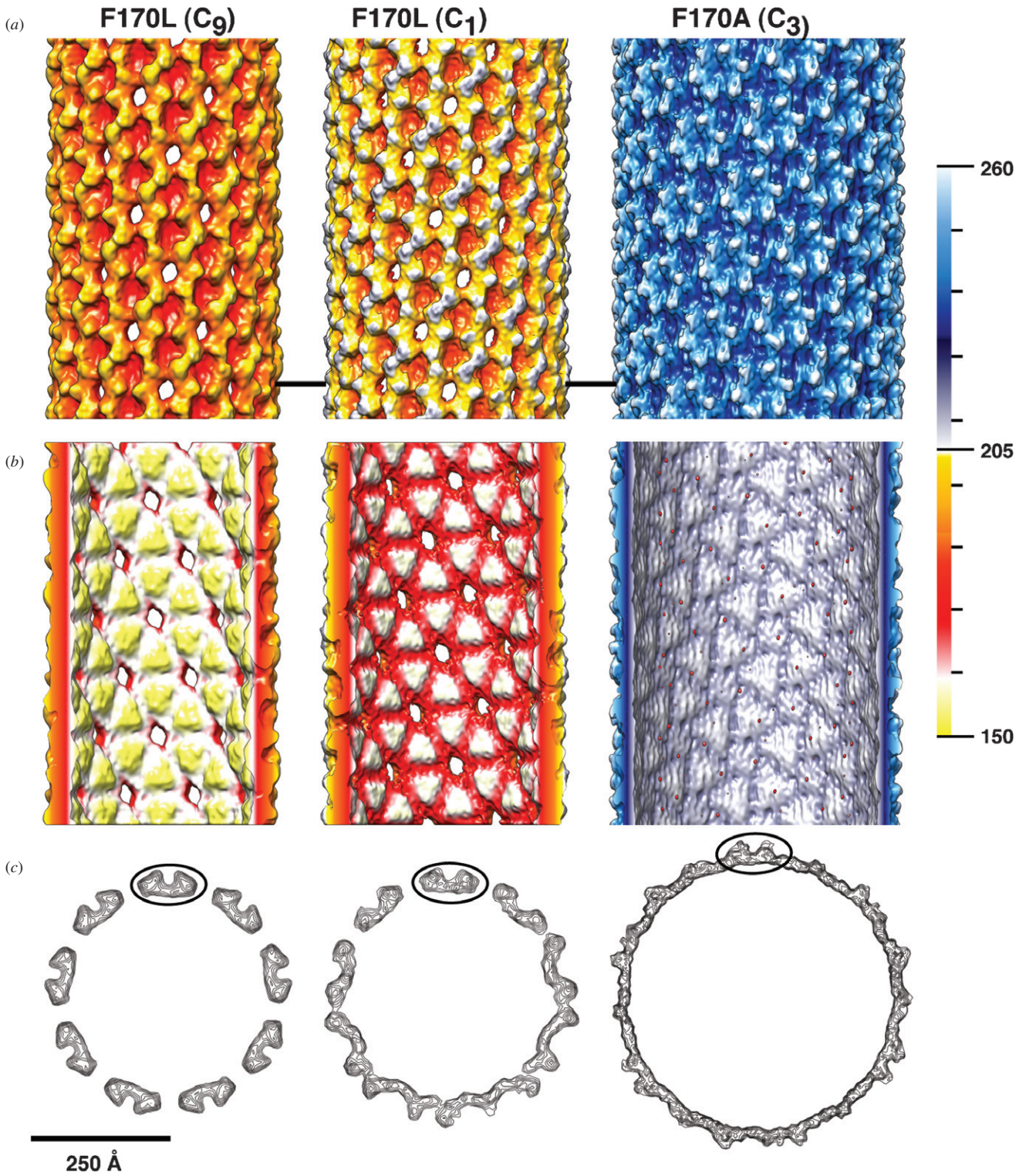

Figure 4. Cryo-reconstructions of C_9, C_1 and C_3 polyheads. (*a*) Radially color-cued, surface-shaded representations of the front halves of all three classes of P22 polyheads show different helical arrangements of hexons. All maps are oriented to align one hexon at the center and bottom of each view as indicated by the black lines. Color bar indicates corresponding radii in Å. (*b*) Same as (*a*), for the back halves of the reconstructions. Trimeric inter-hexon contacts form prominent features on the inside of the C_9 and C_1 forms, but the C_3 form has a smoother inner surface. (*c*) Planar sections (∼5 Å thick) normal to the polyhead axes, generated by the program cplot [66], show differences in polyhead diameter, axial symmetry and wall thickness. Cross-sections through the aligned hexons are circled, and correspond to the level in the maps designated by the black lines in (*a*).

(see the Materials and methods section) to select segments to include in each of the three reconstructions. The number of outliers in the data set of the F170L polyheads with C_9 symmetry (11.5% of segments) was considerably less than that for the F170L polyheads with C_1 symmetry (41.8% of segments) (figure 3). Only 3.4% of the F170A polyheads (C_3

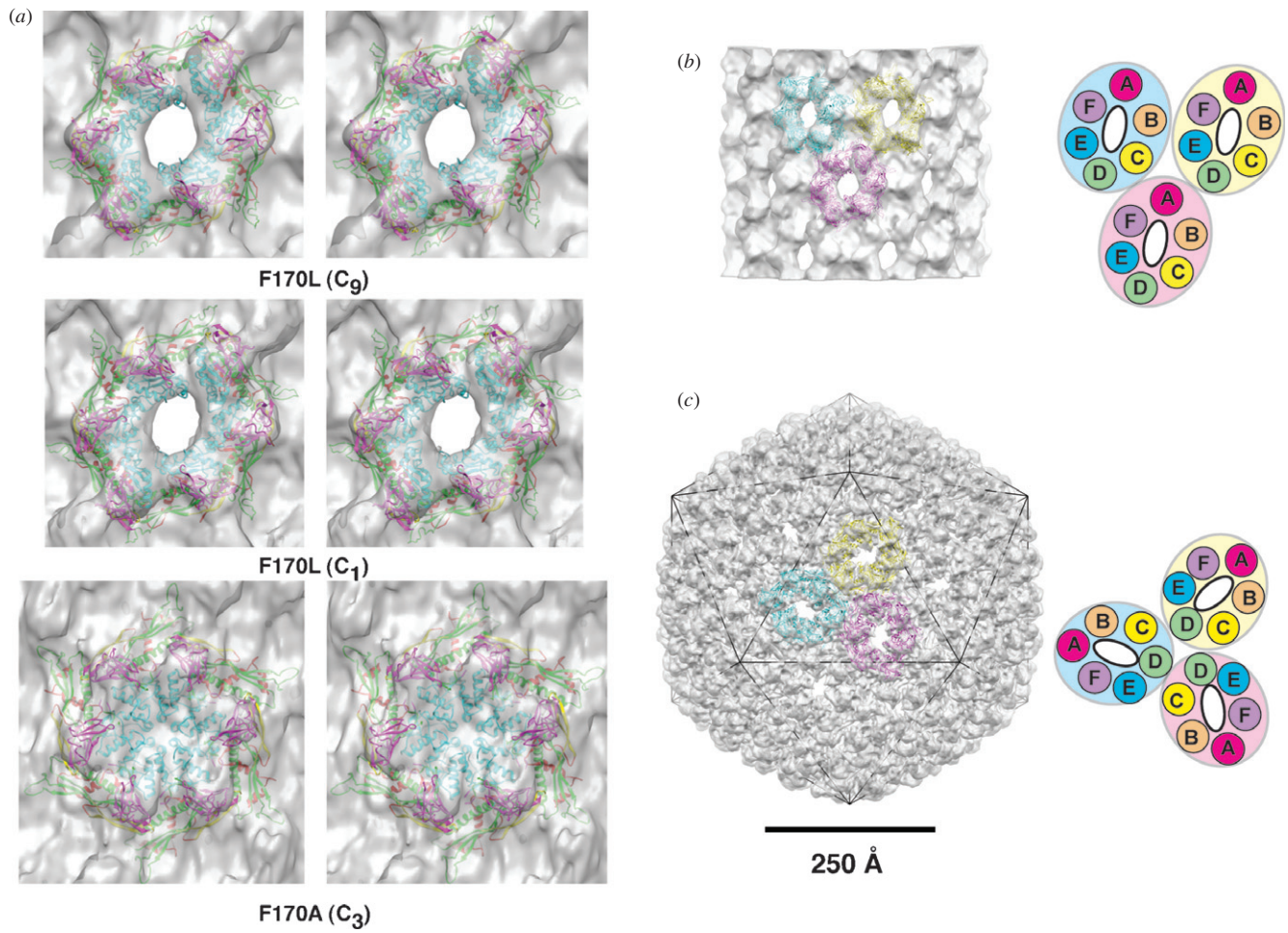

Figure 5. Hexon organization differs in polyheads and procapsids. (*a*) Stereo images of ribbon models of the hexons color-coded by domain as in figure 1(*a*), fit into the three polyhead density maps [26]. The procapsid form of the hexon was docked into F170L C_9 and C_1 structures, and the mature form of the hexon was docked into the F170A C_3 density map. (*b*) Same as (*a*), but showing a larger region of the map with the fit of three neighboring hexons, each distinguished by a different color. The schematic diagram on the right, with each subunit emphasized in a different color, shows that the skewed hexons are all identically oriented relative to the helix axis. The F170L C_9 polyhead is shown as a representative example, but all three polyheads display similar hexon organization. (*c*) Density map of the P22 procapsid [15] docked with models of three neighboring, skewed hexons, color coded to distinguish subunits around a strict threefold axis. The schematic diagram on the right shows that the skewed hexons are arranged with strict threefold symmetry.

symmetry) were identified as outliers, indicating that these are relatively rigid, uniform structures (figure 3).

All P22 polyheads contain CP hexons

Analysis of the incoherently averaged power spectra for each type of polyhead, coupled with measurements of the diameter of each polyhead segment, provided the means to initially estimate the rotation ($\Delta\varphi$) and the axial rise (ΔZ) per subunit for the different helical lattices. For one class of polyhead (F170A), layer line intensities were observed at spacings as fine as 9.6 Å in the average transform (data not shown). We used the estimates of the $\Delta\varphi$ and ΔZ parameters and a featureless, hollow cylinder or a random model as initial input to the IHRSR++ program (figure 4). Both of these initial models led to essentially identical, final reconstructed density maps, indicating that the choice of model did not bias the result.

Shaded-surface representations of each of the polyhead maps clearly reveal the arrangements of hexons in the respective helical lattices (figure 4(*a*)). Though most of the polyheads we examined were comprised solely of hexagons, some were capped (data not shown). This indicates that pentons can be incorporated at the ends of polyheads, and when they are, the helical lattice is disrupted and terminated. Capping of polyhead ends can occur in the absence of portal protein, since F170L polyheads are formed *in vitro* from purified CP. Both F170L polyheads have skewed hexons, whereas the F170A polyhead has isometric hexons. The interior surface of the F170A polyhead is relatively smooth in comparison to the prominent features on the inner surfaces of both types of F170L polyheads, which arise from trimeric inter-subunit and inter-hexon contacts (figure 4(*b*)). These interactions likely dictate the conformational switching that occurs in the CP subunits, because scaffolding protein binding is believed to occur at trimer sites in the procapsid [16, 17]. Planar sections, ∼5 Å thick and normal to each polyhead

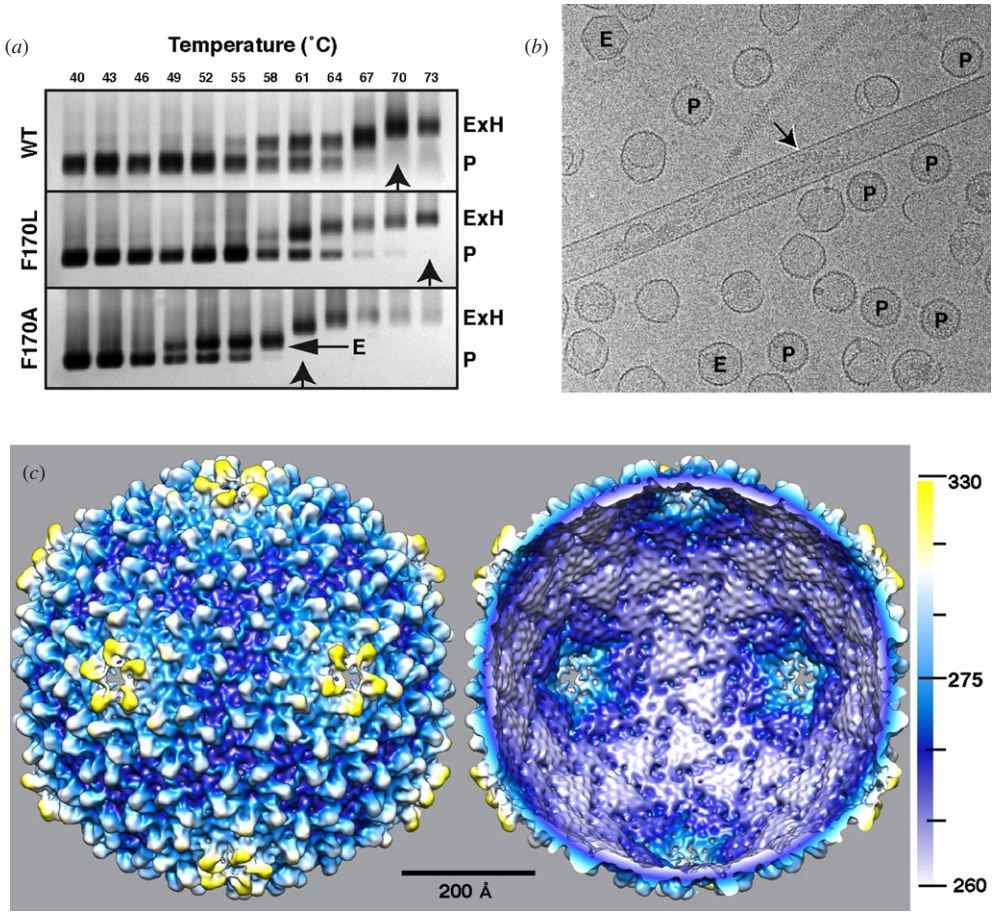

Figure 6. Unheated F170A expanded heads retain their pentons. (*a*) Agarose gel of procapsids treated at different temperatures (see the Materials and methods section). The vertical arrows indicate the minimum temperature required to induce 100% of procapsids (P) to expand first into structures that retain the pentons (E) and then into penton-less particles (ExH). Horizontal arrow points to expanded particles that retain their pentons. (*b*) Micrograph of vitrified F170A particles isolated from phage-infected cells. Labels identify the polyhead (arrow) and several procapsids (P) and expanded particles (E). (*c*) Radially color-cued, surface-shaded representation of the F170A expanded head (particles labeled 'E' in (*b*)) cryo-reconstruction. Color bar indicates corresponding radii in Å.

axis, highlight the different axial symmetries (figure 4(*c*)). The cross section through the C_9 polyhead shows nine, U-shaped features corresponding to identical slabs through the symmetry-related hexons at a level corresponding to the black line in figure 4(*a*). The cross sectioned view of the C_1 polyhead captures only one hexon (encircled) slabbed at the same level as those in the C_9 polyhead: all others around the circumference represent slabs through different portions of the hexon. The wall of the C_3 polyhead is much thinner than that in the C_9 or C_1 polyhead, and the profiles of the slabbed hexon (encircled) and the other two, threefold-related hexons, clearly show a dramatic change in hexon morphology corresponding to its conversion to the expanded state.

Hexon structure differs between F170L and F170A polyheads

The hexons in both types of F170L polyhead (C_9 and C_1) are similar to the hexons in the procapsid (immature) form of the virus (figure 5(*a*)). Indeed, the subunits adopt a skewed arrangement about a large, asymmetric hole. In sharp contrast, the hexons in F170A polyheads are similar to hexons in the mature virion as they are nearly isometric, with local sixfold symmetry, and the axial holes are occluded by the A-domains of the CP subunits (figure 1). The recently derived pseudo-atomic models of the immature and mature forms of the WT hexons [15] were docked as rigid bodies into all three polyhead cryo-reconstructions using Chimera [26]. The unmodified model of the immature hexon (PDB accession 3IYI) fits best into the two F170L polyhead reconstructions, whereas the unmodified model of the mature hexon (PDB accession 3IYH) fits best into the F170A polyhead map (figure 5(*a*)). Discrepancies between these hexon models and the density envelopes may in part be a consequence of the limited resolutions of the reconstructions. Though we did fit individual subunits into the density maps, we deemed this process to be unreliable.

Though the hexons in polyheads clearly resemble the capsomers in procapsids and mature virions, the hexon:hexon interactions in polyheads totally differ from those in isometric particles (figures 5(*b*) and (*c*)). Hexons are related by threefold symmetry in icosahedral, $T = 7$ particles, but in each polyhead, the hexons are all identically oriented relative to the helix axis. This distinction in the packing of hexons in spherical

and cylindrical particles is most obvious in particles with skewed hexons (figures 5(*b*) and (*c*)). Such obvious differences in hexon orientation must be a consequence, at least in part, of the different interactions at the capsomer:capsomer interface that are dictated by scaffolding protein binding (figure 1).

F170A procapsids expand readily in vitro

F170L procapsid shells are more resistant to expansion *in vitro* than WT shells [13]. *In vitro* expansion of procapsids or procapsid shells requires either heat or chemical treatment [29, 30]. Both cause WT procapsids to form pentonless, expanded heads (ExH), which are particles that mimic mature virions with regard to hexon arrangement and structure [15, 31]. To quantify the minimum energy needed to expand 100% of a procapsid sample (vertical arrows in figure 6(*a*)), we heated procapsids comprising F170L, F170A and WT CPs at temperatures ranging from 40 to 73 °C (see the Materials and methods section) and examined the products by agarose gel electrophoresis as described previously [31] (figure 6(*a*)). F170A and WT procapsids were completely absent at 61 and 70 °C, respectively. Temperatures exceeding ∼67 °C lead to penton release for WT CP, as signified by a change in agarose gel mobility. F170L procapsids required the highest temperature (73 °C) to induce complete expansion. Hence, alanine or leucine substitutions for phenylalanine at residue 170 affect maturation oppositely: procapsids with alanine expand more readily and those with leucine less readily relative to WT procaspids.

Three distinct types of particles were observed in images of vitrified F170A assembly products that were purified from unheated phage-infected cells. These included polyheads, procapsids and expanded heads that retained their pentons (figure 6(*b*), 'E'). The expanded F170A procapsids accounted for ∼20% of the total number of particles. In contrast, spontaneously expanded WT or F170L procapsids were not observed in samples treated by the same methods (data not shown). A cryo-reconstruction of 'E' particles revealed hexons of similar morphology to those in F170A polyheads (figure 6(*c*)). Spontaneous expansion of some F170A procapsids suggests that F170A polyheads first assemble in an unstable, immature state comprising skewed hexons and then rapidly convert to an expanded, mature form, with hexons adopting the symmetric morphology. This conversion, though yet to be verified experimentally, seems likely given that the CPs in P22 and related phage have never been observed to assemble directly into mature particles. Differential scanning calorimetry experiments show that scaffolding proteins reversibly exit from WT procapsids beginning at temperatures as low as 37 °C, with about half lost at 44.5 °C and all lost at temperatures approaching 50 °C [30]. Given that F170A expansion begins at ∼49 °C (figure 6(*a*), horizontal arrow), scaffolding protein interactions may stabilize the immature form of the capsid.

Conclusions and outlook

Variations at CP residue 170 affect P22 assembly

The β-hinge in the P22 CP, which includes residue F170, is the most dynamic region of the subunit during capsid maturation [11, 32, 33]. This hinge appears to direct motion of the A-domain during hexon symmetrization that occurs simultaneously with expansion [11]. However, in spite of β-hinge variations induced by amino acid substitutions [14], difference maps between cryo-reconstructions of WT and F170 variant procapsid shells showed only subtle perturbations in the overall hexon structure (secondary structure elements were within ∼6 Å of their WT positions). The F170A-WT procapsid shell difference map indicated that the most dramatic changes occurred near the fivefold axes of symmetry, and these were attributed to an increase in rigidity of the CP at the center of the F170A pentons [14]. However, the F170L-WT procapsid shell difference map showed no changes, including subtle ones, as the two maps were essentially identical to the limits of resolution of the data. F170A CP binds more weakly to the scaffolding protein than does the WT, F170K or F170L CPs. Consequently, F170A polyheads form even in the presence of scaffolding proteins, and F170A procapsids expand with minimal thermal input. F170L CPs bind scaffolding proteins at near-WT levels, and, as expected, F170L polyheads do not form in the presence of scaffolding proteins and procapsids require more energy than WT shells to expand [14].

P22 assembly occurs by addition of CP monomers [34]. This type of assembly mechanism is distinct from related dsDNA phages such as HK97 [35, 36] and T4 [37] as well as more divergent viruses such ϕX174 [38] and the human papilloma viruses [39], all of which assemble from preformed capsomers. Neglecting the presence of portals in P22, the capsid has $T = 7$, icosahedral lattice symmetry and exhibits quasi-equivalence as originally proposed by Capsar and Klug [40]. The asymmetric unit of the $T = 7$ capsid contains seven, quasi-equivalent CPs: six in a hexon and one in a penton. CPs are still assembled into hexons when P22 polyheads form in the absence of scaffolding proteins. Scaffolding proteins may be more important for dictating proper interactions between capsomers. This is consistent with the putative location of scaffolding-binding sites at quasi and strict threefold symmetry axes and with the observation that, in the absence of scaffolding proteins, WT CPs form a significant population of $T = 4$ icosahedral particles, along with some $T = 7$ particles and spirals [16, 17, 41]. In a $T = 4$ particle, hexons are centered at the strict twofold symmetry axes, and hence the threefold-related hexon:hexon interactions differ from a $T = 7$ structure (figure 7(*a*)). Scaffolding protein interactions with CPs likely affect P22 assembly in multiple ways. These interactions seem to be crucial for CPs to be assembled into pentons and to assure proper curvature of the shell. They may also help stabilize procapsids and prevent premature expansion in a manner similar to that proposed for stabilization of T7 procapsids [42]. Based on current evidence, we believe that scaffolding protein:CP interactions drive the formation of specific, trimeric CP associations (see below).

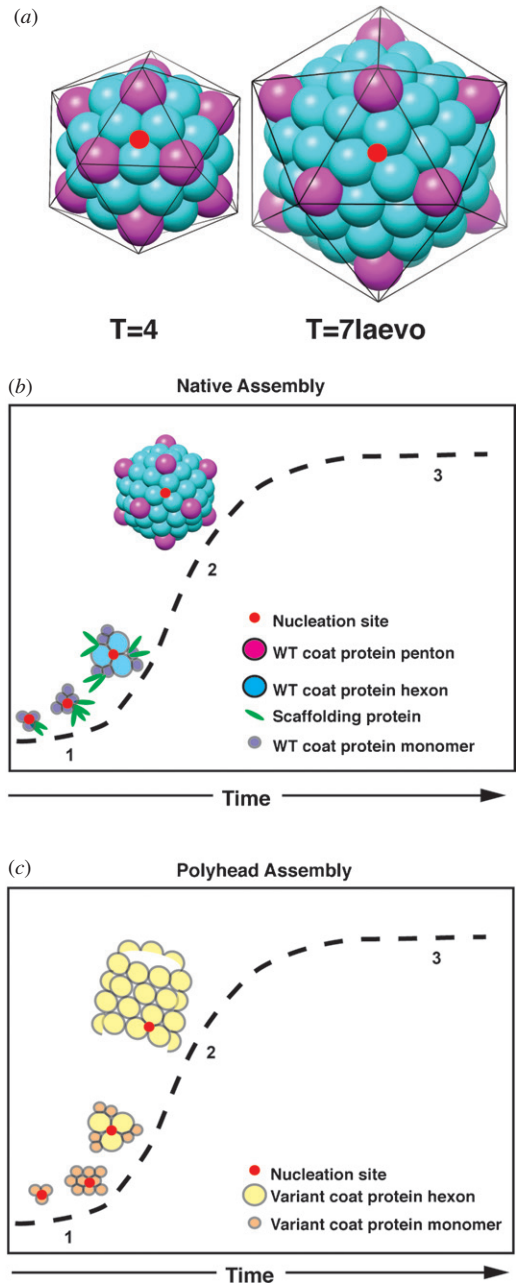

Figure 7. Capsid and polyhead assembly. (*a*) Organization of $T = 4$ and $T = 7$ icosahedral particles with hexons depicted as cyan spheres and pentons as magenta spheres. (*b*) Kinetic plot of a typical *in vitro* assembly pathway for WT CPs [45]. Step 1: nucleation and filling the pipeline with intermediates. Step 2: growth phase and completion of some particles. Step 3: slow asymptotic approach to equilibrium. (*c*) Same as (*b*), but for variant CP that forms polyheads. The ordinate axes for (*b*) and (*c*) represent a proposed progress of assembly.

Nucleation of P22 assembly involves formation of trimeric CP interactions

Many dsDNA tailed phages and herpes viruses first assemble into metastable, precursor capsids that adopt a roughly spherical shape, where curvature of the capsid is approximately uniform in all directions (positive Gaussian curvature) [43]. The presence of CPs alone is often insufficient to direct the assembly of correctly sized, spherical capsids. Additional proteins, frequently scaffolding proteins, are often required to establish proper curvature and hence capsid size [43, 44]. Thus, regulation of capsid size and morphology depends on proper interactions between CPs and scaffolding proteins. For P22, nucleation is directly affected by anion concentration [45]. At low ionic strength, more nuclei than normal are formed ('over-nucleation'), and these lead to abortive, half-capsids, which have the same curvature as native particles. This can be confirmed, since addition of CP to these half capsids leads to $T = 7$ particles [45]. Thus, nucleation rate alone does not change P22 capsid geometry. However, the complete absence of P22 scaffolding proteins results in aberrant capsids, the most common of these being icosahedral, $T = 4$ capsids, which highlights the fact that scaffolding proteins have both structural and catalytic roles during assembly [41]. The F170 variants we have characterized in this study have altered scaffolding binding capacity and produce some structures with zero Gaussian curvature (helical cylinders). We conclude, therefore, that scaffolding proteins impose positive Gaussian curvature in CP:CP interactions necessary for forming the $T = 7$ procapsid shell.

Portals (also called 'connectors') often act as nucleation sites for capsid assembly as has been demonstrated for dsDNA phage like ϕ29 [46, 47]. In other phages such as T4 [48] and λ [49, 50], WT CPs assemble into polyheads when the portal is absent or the portal gene is mutated, and this 'nucleation failure' has been cited as the cause for polyhead formation [43]. Improper nucleation may likewise lead to polyhead formation in P22, but in a manner unrelated to portal incorporation. We suggest that procapsid assembly in P22 is nucleated by scaffolding proteins, which mediate the formation of trimeric CP interactions that generate intercapsomer contacts necessary to produce a closed, $T = 7$ structure.

Several lines of evidence indicate that the portal complex is not required for nucleation of P22 assembly. First, the assembly rate *in vivo* remains the same when the portal is absent [51]. Second, *in vitro* assembly of CPs in the presence of scaffolding proteins alone yields procapsid-like particles with the same morphology as procapsids in WT infections, and these particles form with very high fidelity (~80% of particles have correct geometry) despite the absence of portals [52]. Third, mutations in the P22 portal gene do not cause polyheads to form [51]. If the portal protein is over-expressed, two or three portals can be incorporated into P22 procapsids [53]. In addition, a single amino acid substitution in the P22 CP yields two-tailed phage (Suhanovsky *et al* unpublished data [14]). Together, these data suggest that portals can be incorporated during the growth phase of assembly. Likewise, for bacteriophage T7, prohead assembly proceeds by formation of an incomplete shell, followed by insertion of the core–connector complex, thus indicating that portals are not required for nucleation of some capsids [54]. Finally, structural studies of $T = 7$ and $T = 4$ procapsids formed from P22 WT CPs showed that the penton:hexon interactions appear to be very similar and suggested that the portal complex does not establish initial shell curvature [41]. Though it remains an open question

whether portals can also nucleate P22 assembly, they are certainly not required. This then raises the question of how curvature is regulated if initiation of assembly does not occur at a unique vertex. The different sets of intercapsomer contacts observed in P22 polyheads versus procapsids (figures 5(*b*) and (*c*)) suggest that nucleation of proper P22 assembly begins with CP:scaffolding protein interactions that stabilize threefold symmetric associations among CPs.

Hexon skew and capsid maturation is independent of icosahedral symmetry

Precursor capsids in P22 [55], T7 [56], λ [57], HK97 [35] and herpes simplex 1 [58] employ skewed hexons to accommodate changes in curvature that occur during the transition from a spherical to polyhedral shape [43]. In P22 the hexons contain a large axial hole that likely provides the site through which scaffolding proteins exit as the genome is packaged [59]. The determinant of hexon skew is unknown, but several different mechanisms have been proposed. For bacteriophage $\phi 29$, studies of isometric $T = 3$ and $T = 4$ particles indicate that scaffolding protein binding induces hexon skew [60]. Alternatively, studies of a variant HK97 CP that forms 'whiffleball' structures (mature, pentonless capsids) revealed that hexon skew is induced by an initial hexon:penton interaction that occurs when proheads assemble [61]. In addition, these mutant HK97 hexons are inherently more stable than mutant pentons, since there is a dramatic shift in the ratio of preformed capsomers in solution (i.e. the mutant HK97 CP favors the formation of hexons over pentons when compared to WT CP *in vitro*) [61]. In P22, hexon skew occurs even when CP assembles into isometric $T = 7$ and $T = 4$ capsids in the absence of scaffolding [41]. As reported here, though P22 hexons are packed differently in polyheads compared to isometric procapsid shells, they are skewed in both F170L structures. The same is true for hexons in SPO1 polyheads [4]. Therefore, hexon skew in P22 does not require hexons to interact with pentons or scaffolding proteins, and skew may instead be an inherent property of the CP structure.

P22 polyheads, just like those in λ [62], T4 [63] and T7 [2], have been observed to include hexons in the mature, isometric form. Thus, hexons can expand and mature regardless of the interactions that they have with each other, with the portal complex, or with pentons as evidenced by polyheads and isometric $T = 7$ and $T = 4$ particles. T4 and λ polyheads bind head stabilization (hoc/soc) and decorator (gpD) proteins, and these proteins only recognize and bind structures that have matured [63, 64]. Unlike T4 and λ, P22 needs no auxiliary proteins to provide stability in the mature heads. However, phage L, a close relative of P22, does employ two types of decorator protein [65]. One of these (Dec) binds only at the quasi threefold axes of symmetry in mature P22 heads [65], indicating that it detects the difference in capsid quaternary structure. Whether Dec binds to P22 polyheads has yet to be determined, but is the subject of current investigations.

Accession numbers

Density maps of the C_9 (EMD-1751), C_1 (EMD-1746) and C_3 (EMD-1747) polyheads are deposited at the Electron Microscopy Data Bank.

Acknowledgments

We thank N H Olson for expert guidance in cryo-TEM, K and J Pogliano (University of California, San Diego) for use of their lab space and equipment during sample generation, and J E Johnson (TSRI) for helpful discussions. This work was supported in part by NIH grants R37 GM-033050 and 1S10 RR-020016 to TSB, EB001567 to EHE and GM-076661 to CMT, by NIH fellowship F32A1078624 to KNP, and support from UCSD and the Agouron Foundation to TSB.

References

[1] Krupovic M and Bamford D H 2008 Virus evolution: how far does the double beta-barrel viral lineage extend? *Nat. Rev. Microbiol.* **6** 941–8
[2] Steven A C, Serwer P, Bisher M E and Trus B L 1983 Molecular architecture of bacteriophage T7 capsid *Virology* **124** 109–20
[3] Steven A, Couture E, Aebi U and Showe M 1976 Structure of T4 polyheads: II. A pathway of polyhead transformation as a model for T4 capsid maturation *J. Mol. Biol.* **106** 187–221
[4] Parker M L, Ralston E J and Eiserling F A 1983 Bacteriophage SPO1 structure and morphogenesis: II. Head structure and DNA size *J. Virol.* **46** 250–9
[5] Georgopoulos C P, Hendrix R W, Casjens S R and Kaiser A D 1973 Host participation in bacteriophage lambda head assembly *J. Mol. Biol.* **76** 45–60
[6] Bancroft J B, McDonald J G and Rees M W 1976 A mutant of cowpea chlorotic mottle virus with a perturbed assembly mechanism *Virology* **75** 293–305
[7] Byeon I J *et al* 2009 Structural convergence between cryo-EM and NMR reveals intersubunit interactions critical for HIV-1 capsid function *Cell* **139** 780–90
[8] Li S, Hill C P, Sundquist W I and Finch J T 2000 Image reconstructions of helical assemblies of the HIV-1 CA protein *Nature* **407** 409–13
[9] Baker T S, Caspar D L and Murakami W T 1983 Polyoma virus 'hexamer' tubes consist of paired pentamers *Nature* **303** 446–8
[10] Lepault J, Petitpas I, Erk I, Navaza J, Bigot D, Dona M, Vachette P, Cohen J and Rey F A 2001 Structural polymorphism of the major capsid protein of rotavirus *EMBO* **20** 1498–507
[11] Teschke C M and Parent K N 2010 'Let the phage do the work': using the phage P22 coat protein structure as a framework to understand its folding and assembly mutants *Virology* **401** 119–30
[12] Earnshaw W and King J 1978 Structure of phage P22 coat protein aggregates formed in the absence of the scaffolding protein *J. Mol. Biol.* **126** 721–47
[13] Parent K N, Suhanovsky M M and Teschke C M 2007 Polyhead formation in phage P22 pinpoints a region in coat protein required for conformational switching *Mol. Micro.* **65** 1300–10
[14] Suhanovsky M M, Parent K N, Dunn S E, Baker T S and Teschke C M 2010 Determinants of bacteriophage P22 polyhead formation: the role of coat protein flexibility in conformational switching *Mol. Micro.* submitted

[15] Parent K N, Khayat R, Tu L H, Suhanovsky M M, Cortines J R, Teschke C M, Johnson J E and Baker T S 2010 P22 coat protein structures reveal a novel mechanism for capsid maturation: stability without auxiliary proteins or chemical crosslinks *Structure* **18** 390–410

[16] Thuman-Commike P A, Greene B, Malinski J A, Burbea M, McGough A, Chiu W and Prevelige P E J 1999 Mechanism of scaffolding-directed virus assembly suggested by comparison of scaffolding-containing and scaffolding-lacking P22 procapsids *Biophys. J.* **76** 3267–77

[17] Thuman-Commike P A, Greene B, Jakana J, McGough A, Prevelige P E and Chiu W 2000 Identification of additional coat-scaffolding interactions in a bacteriophage P22 mutant defective in maturation *J. Virol.* **74** 3871–3

[18] Egelman E 2000 A robust algorithm for the reconstruction of helical filaments using single-particle methods *Ultramicroscopy* **85** 225–34

[19] Baker T S, Olson N H and Fuller S D 1999 Adding the third dimension to virus life cycles: three-dimensional reconstruction of icosahedral viruses from cryo-electron micrographs *Microbiol. Mol. Biol. Rev.* **63** 862–922
Baker T S, Olson N H and Fuller S D 2000 Adding the third dimension to virus life cycles: three-dimensional reconstruction of icosahedral viruses from cryo-electron micrographs *Microbiol. Mol. Biol. Rev.* **64** 237 (erratum)

[20] Ludtke S J, Baldwin P R and Chiu W 1999 EMAN: semiautomated software for high-resolution single particle reconstructions *J. Struct. Biol.* **128** 82–97

[21] Frank J, Radermacher M, Penczek P, Zhu J, Li Y, Ladjadj Y and Leith A 1995 SPIDER and WEB: processing and visualization of images in 3D electron microscopy and related fields *J. Struct. Biol.* **116** 190–9

[22] Yan X, Dryden K A, Tang J and Baker T S 2007 *Ab initio* random model method facilitates 3D reconstruction of icosahedral particles *J. Struct. Biol.* **157** 211–25

[23] van Heel M and Schatz M 2005 Fourier shell correlation threshold criteria *J. Struct. Biol.* **151** 250–62

[24] Yan X, Sinkovits R S and Baker T S 2007 AUTO3DEM—an automated and high throughput program for image reconstruction of icosahedral particles *J. Struct. Biol.* **157** 73–82

[25] Bowman V D, Chase E S, Franz A W, Chipman P R, Zhang X, Perry K L, Baker T S and Smith T J 2002 An antibody to the putative aphid recognition site on cucumber mosaic virus recognizes pentons but not hexons *J. Virol.* **76** 12250–8

[26] Goddard T D, Huang C C and Ferrin T E 2007 Visualizing density maps with UCSF chimera *J. Struct. Biol.* **157** 281–7

[27] Serwer P and Pichler M E 1978 Electrophoresis of bacteriophage T7 and T7 capsids in agarose gels *J. Virol.* **28** 917–28

[28] Fuller M T and King J 1981 Purification of the coat and scaffolding protein from procapsids of bacteriophage P22 *Virology* **112** 529–47

[29] Earnshaw W, Casjens S and Harrison S C 1976 Assembly of the head of bacteriophage P22: x-ray diffraction from heads, proheads and related structures *J. Mol. Biol.* **104** 387–410

[30] Galisteo M L and King J 1993 Conformational transformations in the protein lattice of phage P22 procapsids *Biophys. J.* **65** 227–35

[31] Teschke C M, McGough A and Thuman-Commike P A 2003 Penton release from P22 heat-expanded capsids suggests importance of stabilizing penton–hexon interactions during capsid maturation *Biophys. J.* **84** 2585–92

[32] Kang S and Prevelige P E Jr 2005 Domain study of bacteriophage p22 coat protein and characterization of the capsid lattice transformation by hydrogen/deuterium exchange *J. Mol. Biol.* **347** 935–48

[33] Lanman J, Tuma R and Prevelige P E Jr 1999 Identification and characterization of the domain structure of bacteriophage P22 coat protein *Biochemistry* **38** 14614–23

[34] Prevelige P E Jr, Thomas D and King J 1993 Nucleation and growth phases in the polymerization of coat and scaffolding subunits into icosahedral procapsid shells *Biophys. J.* **64** 824–35

[35] Conway J F, Duda R L, Cheng N, Hendrix R W and Steven A C 1995 Proteolytic and conformational control of a virus capsid maturation: the bacteriophage HK97 system *J. Mol. Biol.* **253** 86–99

[36] Duda R L, Hempel J, Michel H, Shabanowitz J, Hunt D and Hendrix R W 1995 Structural transitions during bacteriophage HK97 head assembly *J. Mol. Biol.* **247** 618–35

[37] Stortelder A, Hendriks J, Buijs J B, Bulthuis J, Gooijer C, Van Der Vies S M and Van Der Zwan G 2006 Hexamerization of the bacteriophage T4 capsid protein gp23 and its W13V mutant studied by time-resolved tryptophan fluorescence *J. Phys. Chem.* B **110** 25050–8

[38] Tonegawa S and Hayashi M 1970 Intermediates in the assembly of ΦX174 *J. Mol. Biol.* **48** 219–42

[39] Sapp M, Volpers C, Muller M and Streeck R E 1995 Organization of the major and minor capsid proteins in human papillomavirus type 33 virus-like particles *J. Gen. Virol.* **76** (Pt 9) 2407–12

[40] Caspar D L D and Klug A 1962 Physical principles in the construction of regular viruses *Cold Spring Harb. Symp. Quant. Biol.* **27** 1–24

[41] Thuman-Commike P A, Greene B, Malinski J A, King J and Chiu W 1998 Role of the scaffolding protein in P22 procapsid size determination suggested by $T = 4$ and $T = 7$ procapsid structures *Biophys. J.* **74** 559–68

[42] Agirrezabala X, Velazquez-Muriel J A, Gomez-Puertas P, Scheres S H, Carazo J M and Carrascosa J L 2007 Quasi-atomic model of bacteriophage T7 procapsid shell: insights into the structure and evolution of a basic fold *Structure* **15** 461–72

[43] Moody M F 1999 Geometry of phage head construction *J. Mol. Biol.* **293** 401–33

[44] Dokland T 1999 Scaffolding proteins and their role in viral assembly *Cell. Mol. Life Sci.* **56** 580–603

[45] Parent K N, Doyle S M, Anderson E and Teschke C M 2005 Electrostatic interactions govern both nucleation and elongation during phage P22 procapsid assembly *Virology* **340** 33–45

[46] Guo P X, Erickson S, Xu W, Olson N, Baker T S and Anderson D 1991 Regulation of the phage phi 29 prohead shape and size by the portal vertex *Virology* **183** 366–73

[47] Fu C Y and Prevelige P E Jr 2009 *In vitro* incorporation of the phage Phi29 connector complex *Virology* **394** 149–53

[48] Epstein R H, Bolle A, Steinberg C M, Kellenberger E, Boy de la Tour E, Chevalley R, Edgar R S, Sussman M, Denhardt G H and Lielausis A 1963 Physiological studies of conditional lethal mutants of bacteriophage T4D *Cold. Spring Harb. Symp. Quant. Biol.* **28** 375–94

[49] Kemp C L, Howatson A F and Siminovitch L 1968 Electron microscope studies of mutants of lambda bacteriophage *Virology* **36** 490–502

[50] Georgopoulos C P, Hendrix R W, Casjens S and Kaiser A D 1973 Host participation in bacteriophage lambda head assembly *J. Mol. Biol.* **76** 45–60

[51] Bazinet C and King J 1988 Initiation of P22 procapsid assembly *in vivo J. Mol. Biol.* **202** 77–86

[52] Fuller M T and King J 1982 Assembly *in vitro* of bacteriophage P22 procapsids from purified coat and scaffolding subunits *J. Mol. Biol.* **156** 633–65

[53] Moore S D and Prevelige P E Jr 2002 Bacteriophage p22 portal vertex formation *in vivo J. Mol. Biol.* **315** 975–94

[54] Cerritelli M E and Studier F W 1996 Assembly of T7 capsids from independently expressed and purified head protein and scaffolding protein *J. Mol. Biol.* **258** 286–98
[55] Thuman-Commike P A, Greene B, Jokana J, Prasad B V V, King J, Prevelige P E Jr and Chiu W 1996 Three-dimensional structure of scaffolding-containing phage P22 procapsids by electron cryo-microscopy *J. Mol. Biol.* **260** 85–98
[56] Agirrezabala X, Martin-Benito J, Caston J R, Miranda R, Valpuesta J M and Carrascosa J L 2005 Maturation of phage T7 involves structural modification of both shell and inner core components *EMBO J.* **24** 3820–9
[57] Dokland T and Murialdo H 1993 Structural transitions during maturation of bacteriophage lambda capsids *J. Mol. Biol.* **233** 682–94
[58] Trus B L, Booy F P, Newcomb W W, Brown J C, Homa F L, Thomsen D R and Steven A C 1996 The herpes simplex virus procapsid: structure, conformational changes upon maturation, and roles of the triplex proteins VP19c and VP23 in assembly *J. Mol. Biol.* **263** 447–62
[59] Prasad B V V, Prevelige P E Jr, Marieta E, Chen R O, Thomas D, King J and Chiu W 1993 Three-dimensional transformation of capsids associated with genome packaging in a bacterial virus *J. Mol. Biol.* **231** 65–74
[60] Choi K H, Morais M C, Anderson D L and Rossmann M G 2006 Determinants of bacteriophage phi29 head morphology *Structure* **14** 1723–7
[61] Li Y, Conway J F, Cheng N, Steven A C, Hendrix R W and Duda R L 2005 Control of virus assembly: HK97 'Whiffleball' mutant capsids without pentons *J. Mol. Biol.* **348** 167–82
[62] Kemp C L 1971 The *in situ* morphological transition of the bacteriophage lambda tubular head-forms *Virology* **44** 569–75
[63] Ross P D, Black L W, Bisher M E and Steven A 1985 Assembly-dependent conformational changes in a viral capsid protein *J. Mol. Biol.* **183** 353–64
[64] Howatson A F and Kemp C L 1975 The structure of tubular head forms of bacteriophage λ: relation to the capsid structure of petite λ and normal λ heads *Virology* **67** 80–4
[65] Tang L, Gilcrease E B, Casjens S R and Johnson J E 2006 Highly discriminatory binding of capsid cementing proteins in bacteriophage L *Structure* **14** 837–45
[66] Egelman E 2007 The iterative helical real space reconstruction method: surmounting the problems posed by real polymers *J. Struct. Biol.* **157** 83–94
[67] Egelman H 2010 Reconstruction of helical filaments ad tubes *Methods Enzymol.* at press